PAPER • OPEN ACCESS

Exact distributions of the maximum and range of random diffusivity processes

To cite this article: Denis S Grebenkov *et al* 2021 *New J. Phys.* **23** 023014

View the article online for updates and enhancements.

PAPER

Exact distributions of the maximum and range of random diffusivity processes

Denis S Grebenkov[1,2] , Vittoria Sposini[2,3] , Ralf Metzler[2,*] , Gleb Oshanin[4] and Flavio Seno[5]

1   Laboratoire de Physique de la Matière Condensée (UMR 7643), CNRS – Ecole Polytechnique, IP Paris, 91128 Palaiseau, France
2   Institute for Physics and Astronomy, University of Potsdam, 14476 Potsdam-Golm, Germany
3   Basque Center for Applied Mathematics, 48009 Bilbao, Spain
4   Sorbonne Université, CNRS, Laboratoire de Physique Théorique de la Matière Condensée (UMR 7600), 4 Place Jussieu, 75252 Paris Cedex 05, France
5   INFN, Padova Section and Department of Physics and Astronomy 'Galileo Galilei', University of Padova, 35131 Padova, Italy
*   Author to whom any correspondence should be addressed.

E-mail: rmetzler@uni-potsdam.de

Abstract

We study the extremal properties of a stochastic process x_t defined by the Langevin equation $\dot{x}_t = \sqrt{2D_t}\,\xi_t$, in which ξ_t is a Gaussian white noise with zero mean and D_t is a stochastic 'diffusivity', defined as a functional of independent Brownian motion B_t. We focus on three choices for the random diffusivity D_t: cut-off Brownian motion, $D_t \sim \Theta(B_t)$, where $\Theta(x)$ is the Heaviside step function; geometric Brownian motion, $D_t \sim \exp(-B_t)$; and a superdiffusive process based on squared Brownian motion, $D_t \sim B_t^2$. For these cases we derive exact expressions for the probability density functions of the maximal positive displacement and of the range of the process x_t on the time interval $t \in (0, T)$. We discuss the asymptotic behaviours of the associated probability density functions, compare these against the behaviour of the corresponding properties of standard Brownian motion with constant diffusivity ($D_t = D_0$) and also analyse the typical behaviour of the probability density functions which is observed for a majority of realisations of the stochastic diffusivity process.

1. Introduction

The statistics of extreme values (EVs) of stochastic processes has been in the focus of extensive research in the mathematical (see, e.g. [1–3]) and physical (see, e.g. [4–15]) literature over several decades. More recently, EV properties have also received attention in the areas of mathematical finance [18, 19] in which stochastic processes represent one of the main components in the modelling of the dynamics of asset prices, of computer science [20, 21], as well as of the analysis of 'records' of different kinds [19, 22, 23]. Apart from 'simple' EV problems asking for the maximum behaviour of a variable, 'dual' EVs of the min-max and max-min families are relevant in game theory [24] or reliability engineering [25], for which a universal Gumbel limit law emerges [26, 27].

Typically, one computes several types of EVs, which are either interrelated or independent of each other, and hence, provide complementary information about the process x_t under consideration. Commonly considered EVs are, for instance, the persistence probability for not crossing the initial value x_0 of the process [10], the related probability that the process does not reach a given threshold or a given point in space up to time t (i.e. the 'survival' probability) [5], or the first-passage time to a given threshold or spatial location [4–10, 13–15]. For one-dimensional processes, one often considers the maximal positive $\mathcal{M}$ or negative $\underline{\mathcal{M}}$ displacements and the range $\mathcal{R}$ (also called the span or the extent) of x_t (here and henceforth

we assume that $x_0 = 0$) on a given time interval[6]:

$$\mathcal{M}_T = \max_{0 \leqslant t \leqslant T} \{x_t\} \geqslant 0, \qquad \underline{\mathcal{M}}_T = -\min_{0 \leqslant t \leqslant T} \{x_t\} \geqslant 0, \qquad \mathcal{R}_T = \mathcal{M}_T + \underline{\mathcal{M}}_T \geqslant 0. \qquad (1)$$

Here T represents the length ('observation time') of the time series x_t under consideration. When a random process x_t evolves on a one-dimensional lattice, the range R defines another important property, namely, the number of distinct visited sites up to time T [28]. We also note that complementary characteristics of extremal values of Brownian motions such as the distribution of times between minima and maxima has been evaluated recently [29, 30].

Knowledge of the EV statistics is conceptually important for the understanding of various facets of the stochastic process x_t and is relevant for diverse physical phenomena and also in applications in finance, sociophysics and biology, since EVs often trigger a particular response of the system. A prominent application is molecular chemical reaction kinetics, in which a diffusing molecule hits a reaction centre [31]. For instance, during gene regulation a protein needs to diffusively search a specific binding site on the cellular DNA [32]. Recent research demonstrated that for typical biochemical situations with extremely low reactant concentrations knowledge beyond mean chemical rates [31] is essential, due to the significant separation of relevant time scales even in simple geometries [33, 34]. Notably, geometry-control of reaction time scales in gene regulation [35, 36] is closely related to the most likely reaction time [33, 34]. We also mention that the knowledge of EVs is often very beneficial for a non-perturbative analysis of complicated functionals of x_t, permitting for a construction of convergent bounds and, hence, for obtaining non-trivial exact results [37–42].

Most of the available analyses pertain to the paradigmatic process of Brownian motion, or to lattice random walks. In particular, the exact probability density function $P_T(M)$ of the maximal positive displacement $\mathcal{M}_T$ of a one-dimensional Brownian motion has already been derived exactly in the early work by Lévy [1]: denoting the diffusion coefficient as D_0 and supposing that $t \in (0, T)$ one has

$$P_T(M) = \frac{1}{\sqrt{\pi D_0 T}} \exp\left(-\frac{M^2}{4 D_0 T}\right), \qquad (2)$$

normalised to the positive semi-axis $M \geqslant 0$, compare figure 1. Subsequently, the probability density function $P_T(R)$ of the range of Brownian motion was obtained [2] (see also [43–45])

$$P_T(R) = \frac{4}{\sqrt{\pi D_0 T}} \sum_{m=1}^{\infty} (-1)^{m+1} m^2 \exp\left(-\frac{m^2 R^2}{4 D_0 T}\right)$$

$$= \frac{16 D_0 T}{R^3} \sum_{m=0}^{\infty} \left(\frac{2\pi^2 (2m+1)^2 D_0 T}{R^2} - 1\right) \exp\left(-\frac{\pi^2 (2m+1)^2 D_0 T}{R^2}\right). \qquad (3)$$

These two series representations are exact and thus equivalent. The series in the first line highlights the asymptotic behaviour in the limit $R \to \infty$, while the one in the second line is appropriate for the analysis in the small-R (or long-T) limit. Note also that while $P_T(M = 0)$ is finite for any finite T, the probability density function $P_T(R)$ abruptly drops to zero when $R \to 0$, see the entire shape in figure 1. Further on, more complicated multivariate joint distributions of maxima, minima and the range were evaluated [7], while correlations between maxima or between values of the range achieved on different time intervals were studied in [46–49]. A remarkable result has recently been obtained for the distribution of the time instant at which the range of Brownian motion first reaches a prescribed value [50]. Concurrently a variety of first-passage phenomena associated with Brownian motion have been analysed using exact approaches [4–13]. On top of this several accurate approximation schemes have been analysed, permitting one to consider first-passage events in rather complicated, experimentally-relevant geometries [51, 52]. However, the progress in the theoretical analysis of EV statistics for more general processes, in particular, other than standard Brownian motion and especially non-Markovian processes, remains limited, and typically only the behaviour of the expected values of the EVs is known [4–10, 13].

In this paper we derive exact compact expressions for the probability density function $P_T(M)$ of the maximal displacement and for the probability density function $P_T(R)$ of the range for three random-diffusivity stochastic processes introduced recently in [53]. In these models, the process x_t evolves in a one-dimensional system according to the Langevin equation

$$\frac{dx_t}{dt} = \sqrt{2 D_0 V(B_t)} \, \xi_t, \quad x_0 = 0, \qquad (4)$$

---

[6] Note that these quantities are related to the caliper size or spanning diameter in polymer physics, where these extension parameters, obtained from projection to a given axis, are used as a proxy for the radius of gyration [16, 17].
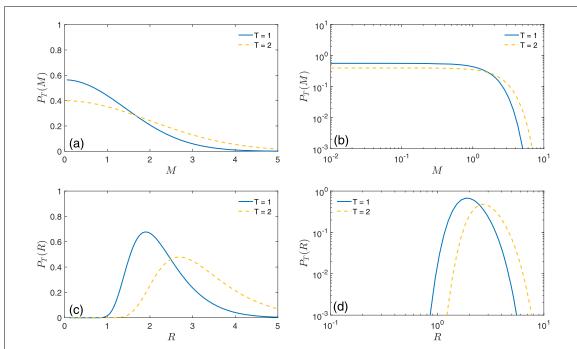
Figure 1. Probability density functions of the extremal behaviour of standard Brownian motion. Panels (a) and (b) show the Gaussian law (2) for the maximum M on linear and log–log scales. Panels (c) and (d) show the probability density (3) for the range. In all panels we depict the functions for the observation times $T = 1$ and $T = 2$. We chose $D_0 = 1$.

where ξ_t is standard white Gaussian noise with zero mean and covariance $\overline{\xi_t \xi_{t'}} = \delta(t - t')$, D_0 is a constant scale factor, and $V(B_t)$ is a dimensionless random diffusivity defined as a functional of independent Brownian motion B_t:

$$B_{t=0} = 0, \qquad \langle B_t \rangle = 0, \qquad \langle B_t B_{t'} \rangle = 2 D_B \min\{t, t'\}, \tag{5}$$

with the diffusivity D_B. Here and henceforth, angular brackets denote averaging with respect to all possible realisations of the Brownian motion B_t, while the overline corresponds to averaging over realisations of the white noise process ξ_t. We note that different versions of the model in (4) corresponding to different choices of the functional $V(B_t)$ have been extensively studied in recent years within the context of diffusion in complex heterogeneous environments [54–65], dynamics of particles involved in polymerisation processes [66, 67] which can be anomalous in the non-Stokesian limit [68], as well as in the mathematical finance literature (see, e.g. [69]). We also mention that stochastically varying diffusivities were identified in simulations of diffusing proteins with fluctuating shape [70], and switching between low and high mobility states was observed in simulations of protein-crowded membranes [71] and the motion of tracer particles in the cytoplasm of mammalian cells [72].

Following [53] we define the three random diffusivity models under study here as follows:

(I) In model I we consider the choice $V(B_t) = \Theta(B_t)$ for the functional V, where $\Theta(x)$ is the Heaviside step function with the property $\Theta(x) = 1$ for $x \geqslant 0$ and zero otherwise. In this model, the process x_t undergoes standard Brownian motion once $B_t > 0$, and it pauses at its current location whenever B_t is negative. Here, the mean-squared displacement $\langle x_t^2 \rangle = D_0 t$ shows Brownian behaviour, however, the diffusion coefficient is smaller by a factor of two than the diffusion coefficient of standard Brownian motion with $V = 1$.

(II) In model II we choose $V(B_t) = \exp(-B_t/a)$, where a is a scale parameter of dimension length. This choice for $V(B_t)$ corresponds to geometric Brownian motion, as assumed for the time evolution of an asset price in the paradigmatic Black–Scholes model [73]. In this model, diffusion is strongly anomalous and the mean squared displacement has an exponential time dependence, $\langle x_t^2 \rangle \sim \exp(t)$.

(III) In model III we choose $V(B_t) = B_t^2/a^2$. Here, the process x_t accelerates when B_t goes away from the origin in either direction, and we are thus facing a superdiffusive behaviour as the process x_t in (4) exhibits a random ballistic growth with time.

We focus here on the generalisation of expressions (2) and (3), derived for Brownian motion, to the above defined three models of random diffusivity. We thus seek the exact expressions for probability density

functions of the maximum and of the range, respectively, defined as

$$P_T(M) = \langle \mathcal{P}_T(M) \rangle, \quad \mathcal{P}_T(M) = \overline{\delta(M - \mathcal{M}_T)} \tag{6}$$

and

$$P_T(R) = \langle \mathcal{P}_T(R) \rangle, \quad \mathcal{P}_T(R) = \overline{\delta(R - \mathcal{R}_T)}, \tag{7}$$

where $\mathcal{P}_T(M)$ and $\mathcal{P}_T(R)$ denote the probability density functions calculated for a given realisation of B_t (and thus a given realisation of diffusivity). We note that the latter realisation-dependent distributions are evidently given by expressions (2) and (3) with $D_0 T$ replaced by the integral $D_0 \int_0^T V(B_t) dt$, implying that $\mathcal{P}_T(M)$ and $\mathcal{P}_T(R)$ are, respectively, a Gaussian function or an infinite sum of Gaussians with random variances. As we proceed to show, the averaging over realisations of B_t can be performed exactly for the three models under study and requires only the knowledge of the moment-generating function $\Upsilon(T; \lambda)$ of the random variable $D_0 \int_0^T V(B_t) dt$,

$$\Upsilon(T; \lambda) = \left\langle \exp\left(-\lambda D_0 \int_0^T V(B_t) dt \right) \right\rangle. \tag{8}$$

This function can indeed be calculated exactly for many cases (see, e.g. [3, 21] and references therein) and, in particular, for the models we study here. We proceed to show that the averaged distributions, i.e. $P_T(M)$ and $P_T(R)$, exhibit a markedly different behaviour, as compared to the distributions in (2) and (3). We will compare these predictions against the estimates of the 'typical' behaviour of these distributions (see, e.g. [74, 75]),

$$P_T^{(typ)}(M) = p \mathcal{N}_M \exp\left(\langle \ln(\mathcal{P}_T(M)/p) \rangle \right), \tag{9}$$

$$P_T^{(typ)}(R) = p \mathcal{N}_R \exp\left(\langle \ln(\mathcal{P}_T(R)/p) \rangle \right), \tag{10}$$

where $\mathcal{N}_M$ and $\mathcal{N}_R$ are normalisation constants, while p is an irrelevant auxiliary parameter of inverse length that is introduced to deal with dimensionless quantities under the logarithm but cancels anyway. We will demonstrate that their functional form is supported by some atypical realisations of the process B_t.

The paper is organised as follows. In section 2 we briefly summarise our main results. In two subsequent sections 3 and 4, we present the details of the derivations of our main results, analyse their asymptotic behaviour and their moments, and also estimate their effective broadness by calculating the coefficients of variation of the respective distributions. Additionally, we compare our analytical predictions with the results of numerical simulations. Section 3 is devoted to the maximum, in section 4 we consider the range. Next, in section 5 for the example of the distribution of the maximum, we will discuss its 'typical' shape which should be observed for a majority of realisations of the process B_t (or for small statistical samples) and demonstrate that the exact form obtained for $P_T(M)$ (and for $P_T(R)$) defined in (6) stems from some atypical realisations of the stochastic diffusivity process. Concluding remarks are provided in section 6.

2. Main results

In this section we summarise our main results for the probability density functions $P_T(M)$ and $P_T(R)$, (6) and (7), for the three models under study. The parameters entering these results were defined above in the description of our models.

2.1. Model I
For model I we find that

$$P_T^{(I)}(M) = \frac{1}{\sqrt{\pi^3 D_0 T}} \exp\left(-\frac{M^2}{8 D_0 T} \right) K_0 \left(\frac{M^2}{8 D_0 T} \right), \tag{11}$$

where $K_0(z)$ is the modified Bessel function of the second kind of the zeroth order. In turn, the exact probability density function $P_T^{(I)}(R)$ can be written in either of two equivalent forms: (i) as we proceed to show, the analysis of the short-R behaviour (i.e. the behaviour of the left tail of the probability density function $P_T(R)$) can be realised from the following expression,

$$P_T^{(I)}(R) = \frac{8}{\pi^2} \sum_{m=0}^{\infty} \frac{1}{(2m+1)^2}$$

$$\times \frac{d^2}{dR^2} \left(R \exp\left(-\frac{\pi^2 (2m+1)^2 D_0 T}{2R^2} \right) I_0 \left(\frac{\pi^2 (2m+1)^2 D_0 T}{2R^2} \right) \right), \tag{12}$$

where $I_0(z)$ is the modified Bessel function of the first kind; (ii) in turn, the behaviour of the right tail is conveniently given by an alternative series expansion,

$$P_T^{(I)}(R) = \frac{4}{\sqrt{\pi^3 D_0 T}} \sum_{m=1}^{\infty} (-1)^{m+1} m^2 \exp\left(-\frac{m^2 R^2}{8 D_0 T}\right) K_0\left(\frac{m^2 R^2}{8 D_0 T}\right). \tag{13}$$

Expressions (12) and (13) are related to each other through the Poisson summation formula.

2.2. Model II

For model II we obtain the following exact expression for the probability density function of the maximum,

$$P_T^{(II)}(M) = \frac{2a}{\sqrt{\pi T \left(D_B M^2 + 4 D_0 a^2\right)}} \exp\left(-\frac{a^2}{D_B T} \mathrm{arcsinh}^2\left(\sqrt{\frac{D_B}{D_0}} \frac{M}{2a}\right)\right). \tag{14}$$

The detailed discussion of its rather unusual asymptotic behaviour is presented in the next section. In turn, the probability density function $P_T^{(II)}(R)$ of the range obeys the exact expression

$$P_T^{(II)}(R) = \frac{\partial^2}{\partial R^2}\left(R \Psi_T^{(II)}(R)\right),$$

$$\Psi_T^{(II)}(R) = \frac{16}{\pi^3} \sum_{m=0}^{\infty} \frac{1}{(2m+1)^2}$$

$$\times \int_0^{\infty} \exp\left(-\frac{D_B T}{4a^2} z^2\right) \cosh\left(\frac{\pi z}{2}\right) K_{iz}\left(\frac{2\pi(2m+1)a}{R^2}\sqrt{\frac{D_0}{D_B}}\right) dz, \tag{15}$$

where $K_{iz}(x)$ is the modified Bessel function of the second type of purely imaginary order. This latter form is suitable for the analysis of the short-R behaviour (see section 4). An alternative form appropriate for the analysis of the large-R behaviour follows from (15) via the Poisson summation formula and reads

$$P_T^{(II)}(R) = \frac{8a}{\sqrt{\pi T}} \sum_{m=1}^{\infty} \frac{(-1)^{m+1} m^2}{\sqrt{(D_B m^2 R^2 + 4a^2 D_0)}} \exp\left(-\frac{a^2}{D_B T} \mathrm{arcsinh}^2\left(\sqrt{\frac{D_B}{D_0}} \frac{mR}{2a}\right)\right). \tag{16}$$

2.3. Model III

For model III the probability density function of the maximum has the exact form

$$P_T^{(III)}(M) = \frac{a}{\sqrt{8\pi^3 D_0 D_B}\, T} \left|\Gamma\left(\frac{1}{4} + i\frac{aM}{4\sqrt{D_0 D_B}\, T}\right)\right|^2, \tag{17}$$

where $\Gamma(z)$ is the gamma function. The probability density function of the range admits the exact expansion

$$P_T^{(III)}(R) = \frac{8}{\pi^2} \sum_{m=0}^{\infty} \frac{1}{(2m+1)^2} \frac{\partial^2}{\partial R^2}\left(\frac{R}{\cosh^{1/2}\left(2\pi(2m+1)\frac{\sqrt{D_0 D_B}\, T}{aR}\right)}\right), \tag{18}$$

which is suitable in the short-R limit, while the right tail of the distribution can be accessed via an equivalent expansion,

$$P_T^{(III)}(R) = \frac{\sqrt{2}a}{\sqrt{\pi^3 D_0 D_B}\, T} \sum_{m=1}^{\infty} (-1)^{m+1} m^2 \left|\Gamma\left(\frac{1}{4} + i\frac{maR}{4\sqrt{D_0 D_B}\, T}\right)\right|^2. \tag{19}$$

The rest of the paper presents the details of the derivations of our main results and a discussion of their behaviour.

3. Probability density function of the maximal displacement

We present the details of derivations of the exact expressions for the probability density function $P_T(M)$ summarised earlier in section 2. We find it expedient to base our analysis here on the exact expressions for the first-passage time density $H(t|M)$ that was derived for all three models under study in a recent paper [65]. An alternative approach which takes advantage of the moment-generating function (8) will be used later on in section 5 and will permit us to access the typical behaviour of the probability density.

Let $S_T(M)$ denote the survival probability, i.e. the probability that the process x_t, starting at the origin $x_0 = 0$ at $t = 0$, does not reach a point $M > 0$ within the time interval $t \in (0, T)$. This probability can be expressed as

$$S_T(M) = \int_T^\infty H(t|M)\mathrm{d}t, \tag{20}$$

where $H(t|M)$ is the probability density function of the event that the process x_t reached the point M for the first time at the time instant t. As a consequence, the desired probability density function $P_T(M)$, which defines the probability density that the maximal positive displacement of the process x_t within the time interval $t \in (0, T)$ is exactly equal to M obeys

$$P_T(M) = \frac{\mathrm{d}S_T(M)}{\mathrm{d}M} = \int_T^\infty \frac{\mathrm{d}H(t|M)}{\mathrm{d}M}\mathrm{d}t. \tag{21}$$

In the case of standard Brownian motion ($D_t = D_0$) the survival probability $S_T(M) = \mathrm{erf}(M/\sqrt{4D_0 T})$, where $\mathrm{erf}(x)$ is the error function, $H(t|M)$ is the celebrated Levý–Smirnov distribution, and, eventually, $P_T(M)$ is given by (2).

3.1. Model I

For model I the first-passage time density obeys [65]

$$H^{(\mathrm{I})}(t|M) = \frac{M}{\sqrt{4\pi^3 D_0 t^3}}\, \exp\left(-\frac{M^2}{8D_0 t}\right) K_0\left(\frac{M^2}{8D_0 t}\right). \tag{22}$$

Differentiating the latter expression with respect to M, inserting the result into (21) and integrating it over t, we find our compact expression (11). Note that the density in (22) resembles—but is not identical to—the density $P_T^{(\mathrm{I})}(M)$.

Moreover, due to the presence of $K_0(z)$, the distribution of the maximum exhibits a different asymptotic behaviour in the limits of small and large M as compared to behaviour (2) of Brownian motion. From (11) the asymptotic limit $M \to \infty$ produces to leading order

$$P_T^{(\mathrm{I})}(M) \simeq \frac{2}{\pi M}\, \exp\left(-\frac{M^2}{4D_0 T}\right) \quad (M \to \infty), \tag{23}$$

that is, the probability density decreases with M faster, due to the additional factor $1/M$, than expression (2). For the opposite limit $M \to 0$ we find that

$$P_T^{(\mathrm{I})}(M) \simeq \frac{1}{\sqrt{\pi^3 D_0 T}}\left(\ln\left(\frac{16 D_0 T}{M^2}\right) - \gamma\right) \quad (M \to 0), \tag{24}$$

where $\gamma \approx 0.5772$ is the Euler–Mascheroni constant. Expression (24) implies that $P_T^{(\mathrm{I})}(M)$ logarithmically *diverges* in this limit, while expression (2) remains bounded. Overall we observe that the probability density function (11) is shifted towards smaller M values compared to the distribution (2). In particular, the expected (with respect to the distribution in (11)) value of the maximal displacement of the process x_t in model I obeys

$$\overline{\langle \mathcal{M}_T \rangle} = \frac{4}{\pi^{3/2}}\sqrt{D_0 T}, \tag{25}$$

i.e. it grows with T exactly at the same rate as the expected maximum of Brownian motion, $\overline{\mathcal{M}_T^{\mathrm{BM}}} = \frac{2}{\sqrt{\pi}}\sqrt{D_0 T}$, but has a slightly smaller prefactor ($4/\pi^{3/2} \approx 0.72$ while $2/\pi^{1/2} \approx 1.12$). The expression in (25) can be generalised to derive the moments of the maximum of the process x_t for model I of arbitrary, not necessarily integer order $q \geqslant 0$,

$$\overline{\langle \mathcal{M}_T^q \rangle} = \frac{\Gamma^2\left(\frac{q+1}{2}\right)}{\pi \Gamma\left(\frac{q}{2} + 1\right)}(4D_0 T)^{q/2}. \tag{26}$$

From this expression we also derive the coefficient of variation $v_M^{(\mathrm{I})}$ of the distribution (11):

$$v_M^{(\mathrm{I})} = \frac{\sqrt{\overline{\langle \mathcal{M}_T^2 \rangle} - \overline{\langle \mathcal{M}_T \rangle}^2}}{\overline{\langle \mathcal{M}_T \rangle}} = \sqrt{\frac{\pi^3 - 16}{16}} \approx 0.968. \tag{27}$$

By definition, this property measures the relative weight of fluctuations around the mean value. Hence, for model I these fluctuations are of nearly the same order as the expected value itself, such that $P_T^{(\mathrm{I})}(M)$ is *effectively* broad [11, 12]. Note that the distribution of the maximum of a standard Brownian motion, (2),

appears to be somewhat narrower; there, the coefficient of variation $v_M^{(BM)} = \sqrt{(\pi - 2)/2} \approx 0.756$ is smaller than $v_M^{(I)}$.

3.2. Model II

For model II the exact expression for the probability density function of the first-passage time is given by [65]

$$H^{(II)}(t|M) = \frac{a}{\sqrt{\pi D_B t^3}} \operatorname{arcsinh}\left(\frac{M}{2a\sqrt{D_0/D_B}}\right)$$

$$\times \exp\left(-\frac{a^2}{D_B t} \operatorname{arcsinh}^2\left(\frac{M}{2a\sqrt{D_0/D_B}}\right)\right). \tag{28}$$

Again, differentiating (28) over M and integrating the resulting expression over t, we arrive at our result in (14). The small-M asymptotical behaviour of expression (14) obeys

$$P_T^{(II)}(M) \simeq \frac{1}{\sqrt{\pi D_0 T}} \exp\left(-\frac{M^2}{4D_0 T}\right) \quad (M \to 0). \tag{29}$$

Rather surprisingly, this limiting behaviour is exactly the same as that of (2) for the maximum of standard Brownian motion. In contrast, the large-M asymptotic behaviour is very different from that of standard Brownian motion and follows

$$P_T^{(II)}(M) \simeq \frac{2a}{\sqrt{\pi D_B T M}} \exp\left(-\frac{a^2}{D_B T} \ln^2\left(\sqrt{\frac{D_B}{D_0}}\frac{M}{a}\right)\right) \quad (M \to \infty), \tag{30}$$

i.e. the right tail of the distribution $P_T^{(II)}(M)$ is that of a log-normal distribution. In view of such a 'heavy' tail one expects that higher values of M are more likely than in case of a standard Brownian motion.

The moments of the distribution $P_T^{(II)}(M)$ of arbitrary order $q \geqslant 0$ can be obtained by a straightforward integration of expression (14), leading us to

$$\overline{\langle \mathcal{M}_T^q \rangle} = \frac{2}{\sqrt{\pi}} \left(\frac{4a^2 D_0}{D_B}\right)^{q/2} \int_0^\infty \exp\left(-x^2\right) \left[\sinh\left(\frac{\sqrt{D_B T}}{a}x\right)\right]^q dx$$

$$= \left(\frac{a^2 D_0}{D_B}\right)^{q/2} \sum_{n=0}^\infty (-1)^n \binom{q}{n} \exp\left(\frac{D_B T}{4a^2}(q - 2n)^2\right)$$

$$\times \left(1 + \operatorname{erf}\left(\frac{\sqrt{D_B T}}{2a}(q - 2n)\right)\right), \tag{31}$$

where $\binom{q}{n}$ denotes the binomial coefficient. Naturally, when q is an integer the series is truncated at $n = q$, as can be observed directly from the expression in the first line of (31). From (31) we have, in particular,

$$\overline{\langle \mathcal{M}_T \rangle} = \left(\frac{4a^2 D_0}{D_B}\right)^{1/2} \exp\left(\tau/4\right) \operatorname{erf}\left(\sqrt{\tau}/2\right),$$

$$\overline{\langle \mathcal{M}_T^2 \rangle} = \frac{1}{2}\left(\frac{4a^2 D_0}{D_B}\right) \exp\left(\tau\right)\left(1 - \exp\left(-\tau\right)\right),$$

$$\overline{\langle \mathcal{M}_T^3 \rangle} = \frac{1}{4}\left(\frac{4a^2 D_0}{D_B}\right)^{3/2} \exp\left(9\tau/4\right)$$

$$\times \left(\operatorname{erf}\left(3\sqrt{\tau}/2\right) - 3\exp\left(-2\tau\right)\operatorname{erf}\left(\sqrt{\tau}/2\right)\right), \tag{32}$$

and so on. Here we used the notation $\tau = D_B T/a^2$. We observe that in the case of model II there is no unique time scale, in contrast to model I (and also to model III below). This is a direct consequence of the fact that the right tail of $P_T^{(II)}(M)$ decreases with M slower than an exponential function, which gives rise to the behaviour specific to the so-called *strongly* anomalous superdiffusion for which a growth of the moments with time is not characterised by a unique exponent (see, e.g. [76–78]).

The first two expressions in (32) permit us to evaluate the coefficient of variation $v_M^{(II)}$ of the probability density function $P_T^{(II)}(M)$ in (14):

$$v_M^{(II)} = \frac{\sqrt{1 - 2\exp\left(-\tau/2\right)\operatorname{erf}^2(\sqrt{\tau}/2) - \exp(-\tau)}}{\sqrt{2}\operatorname{erf}(\sqrt{\tau}/2)} \exp\left(\tau/4\right). \tag{33}$$

Remarkably, $v_M^{(II)}$ diverges exponentially, $v_M^{(II)} \simeq \exp(\tau/4)/\sqrt{2}$ as $\tau \to \infty$ (i.e. the observation time T tends to infinity). This signifies that moments of arbitrary order are not representative of the actual behaviour and knowledge of the full distribution $P_T^{(II)}(M)$ is crucial.

3.3. Model III

Lastly, for model III the first-passage time density is [65]

$$H^{(III)}(t|M) = \frac{aM}{2\sqrt{2\pi^3 D_0 D_B}\, t^2} \left| \Gamma\left(\frac{1}{4} + \frac{iaM}{4\sqrt{D_0 D_B}\, t} \right) \right|^2. \tag{34}$$

Differentiating this expression with respect to M and integrating over t, we arrive at our result in (17).

For small M, the gamma function in (17) tends to a constant (with corrections of order $O(M^2)$), and hence, one has

$$P_T^{(III)}(M) = \frac{a\,\Gamma^2(1/4)}{\sqrt{8\pi^3 D_0 D_B}\, T} \left(1 + O\left(M^2 \right) \right) \quad (M \to 0). \tag{35}$$

In turn, for $M \to \infty$, the asymptotic behaviour of $P_T^{(III)}(M)$ is given by

$$P_T^{(III)}(M) \simeq \left(\frac{2a}{\pi\sqrt{D_0 D_B}\, TM} \right)^{1/2} \exp\left(-\frac{\pi a}{4\sqrt{D_0 D_B}\, T} M \right) \quad (M \to \infty), \tag{36}$$

i.e. the right tail of the probability density function of the maximal displacement is an exponential function and hence, is also 'heavier' than the Gaussian tail of the corresponding probability distribution of the maximum of standard Brownian motion. Evidently, expression (17) also favours higher values of the maximum M than the probability density function (2).

The moments of the distribution (17) obey

$$\overline{\langle \mathcal{M}_T^q \rangle} = \left(\frac{4\sqrt{D_0 D_B}\, T}{a} \right)^q f_q, \tag{37}$$

where the dimensionless numerical amplitude f_q is given by

$$f_q = \sqrt{\frac{2}{\pi^3}} \int_0^\infty x^q \left| \Gamma\left(\frac{1}{4} + ix \right) \right|^2 dx. \tag{38}$$

We were unable to perform the integral in the latter equation and, hence, to derive an explicit expression for f_q, except for the particular case when q is an even integer, $q = 2n$. In this latter case, f_q is given by

$$f_{2n} = (-1)^n \left(\frac{d^{2n}}{dz^{2n}} \frac{1}{\sqrt{\cosh(z/2)}} \right) \Bigg|_{z=0} = \frac{\mathcal{A}_n}{2^{3n}}, \tag{39}$$

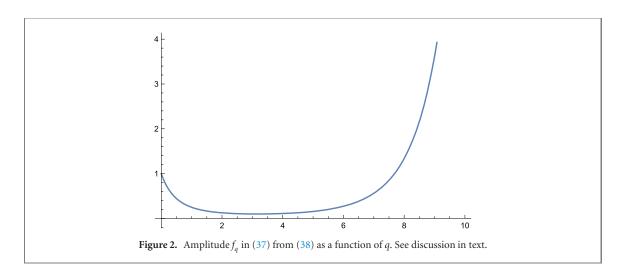where $\mathcal{A}_n$ are integers forming Sloane's sequence A126156 [79]. In particular,

$$f_0 = 1, \qquad f_2 = \frac{1}{8}, \qquad f_4 = \frac{7}{64}, \qquad f_6 = \frac{139}{512}. \tag{40}$$

The numerical factor f_q as a function of q is depicted in figure 2. We realise that f_q turns out to be a non-monotonic function of q. Lastly, we estimate numerically the value of the coefficient of variation of $P_T^{(III)}(M)$ to get

$$v_M^{(III)} \approx 1.012, \tag{41}$$

implying that fluctuations around the mean value of the maximum exceed the latter such that the distribution is effectively broad.

Figure 3 presents the exact probability density functions $P_T(M)$ (solid curves) and their asymptotic forms (dashed and dash-dotted curves) for the three models, highlighting the ranges of validity of the small-M limit as well as the onset of the large-M asymptotic behaviours. The results are shown on both linear and log–log scales, to highlight the asymptotic behaviour as well as the respective crossovers. Note specifically the divergence of $P_T(M)$ in the limit $M \to 0$ for model I.
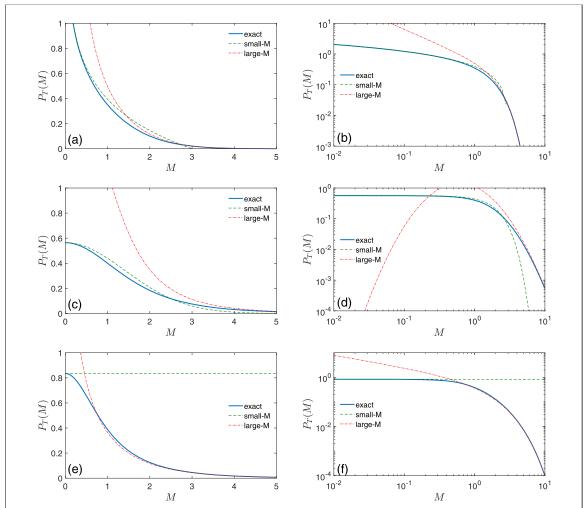
Figure 2. Amplitude f_q in (37) from (38) as a function of q. See discussion in text.

Figure 3. Probability density function $P_T(M)$ of the maximal displacement along with the small-M and large-M asymptotic behaviours for model I (a) and (b), model II (c) and (d), and model III (e) and (f), plotted on linear (a), (c), (e) and log–log (b), (d), (f) scale. We set $D_0 = 1$, $T = 1$, $a = 1$, and $D_B = 1$. Compare this behaviour to the Brownian limit in figure 1.

3.4. Relation between the moments of the maximum and of the random diffusivity

To close this section we present a general relation between the moments of the maximum and the moments of the random variable $D_0 \int_0^T V(B_t)\mathrm{d}t$,

$$\overline{\langle \mathcal{M}_T^q \rangle} = \frac{2^q}{\sqrt{\pi}} \Gamma\left(\frac{q+1}{2}\right) \left\langle \left(D_0 \int_0^T V(B_t)\mathrm{d}t\right)^{q/2} \right\rangle, \tag{42}$$

which holds for arbitrary $q \geqslant 0$. This relation can be proven directly by using the definition in (21) and also a general expression for the first-passage time distribution presented in our previous work [65]. Below we will merely demonstrate the validity of (42) by establishing a relation between the moments of the maximum and the moments of the range. Using the standard 'replica trick' we find the following simple expression that connects the typical behaviour of the maximum and the typical behaviour of the random variable $D_0 \int_0^T V(B_t) \mathrm{d}t$,

$$\overline{\langle \ln(\mathcal{M}_T) \rangle} = \lim_{q \to 0} \frac{1}{q} \left(\overline{\langle \mathcal{M}_T^q \rangle} - 1 \right) = \frac{1}{2} \left\langle \ln \left(D_0 \int_0^T V(B_t) \mathrm{d}t \right) \right\rangle - \frac{\gamma}{2}, \tag{43}$$

where γ is again the Euler–Mascheroni constant. In particular, in the special case $V(B_t) \equiv 1$ (i.e. when the process x_t in (4) is standard Brownian motion), equation (43) reproduces the known result

$$\overline{\ln \left(\mathcal{M}_T^{(\mathrm{BM})} \right)} = \frac{1}{2} \left(\ln(D_0 T) - \gamma \right). \tag{44}$$

4. Probability density function of the range

In this section, we first present the arguments underlying the derivation of $P_T(R)$ and evaluate general expressions which highlight the short-R and large-R behaviour, i.e. the left and right tails of $P_T(R)$, respectively. We then establish a general relation between the moments of the range and the moments of the random variable $D_0 \int_0^t V(B_t) \, \mathrm{d}t$, which also permits us to link the moments of the range and the moments of the maximum in the random diffusivity processes. Lastly, we will concentrate on the particular cases and evaluate the exact forms of $P_T(R)$ for the three models under study.

The probability density function of the range R of the process (4) can be evaluated by writing down the corresponding Fokker–Planck equation for the position probability density function $\Pi(x, t)$ (in which the diffusion coefficient D_t is a random function of time), appropriately rescaling the time variable and then solving the resulting diffusion equation subject to adsorbing boundary conditions. The steps involved in this approach are well described, e.g. in [43–45]. In this procedure we find that $P_T(R)$ can be conveniently represented by two alternative forms, one of which is suitable for the analysis of the small-R behaviour of the probability density function of the range, while the second one is adapted to the large-R asymptotic behaviour.

In the first case $P_T(R)$ is given by

$$P_T(R) = \frac{\partial^2}{\partial R^2} (R \Psi_T(R)), \tag{45}$$

with

$$\Psi_T(R) = \frac{8}{\pi^2} \sum_{m=0}^{\infty} \frac{1}{(2m+1)^2} \Upsilon \left(T; \pi^2 (2m+1)^2 / R^2 \right), \tag{46}$$

and where $\Upsilon(T; \lambda)$ is the moment-generating function which is defined earlier in (8). We note that in virtue of (46) the knowledge of an exact form (8) of $\Upsilon(T; \lambda)$ appears to be the key ingredient for finding exact forms of $P_T(R)$ (see also [62] for the role of this function for the analysis of the first-passage time densities). In turn, the large-λ tail of $\Upsilon(T; \lambda)$ (corresponding to such realisations of B_t when $D_0 \int_0^T V(B_t) \mathrm{d}t$ is small) is responsible for the behaviour of $\Psi_T(R)$ in the limit when $R \to 0$. We proceed to show that such a behaviour can be markedly different depending on how fast $\Upsilon(T; \lambda)$ vanishes when $\lambda \to \infty$. In this sense, the three models under study provide representative examples of different kinds of such a behaviour: in model I the moment-generating function $\Upsilon(T; \lambda)$ vanishes as a power-law when $\lambda \to \infty$ and $P_T(R)$ approaches a constant value as $R \to 0$, while for both models II and III $\Upsilon(T; \lambda) \sim \exp(-\sqrt{\lambda})$ in the leading order in the limit $\lambda \to \infty$, and $\ln P_T(R)$ exhibits a singular behaviour of the form $\ln P_T(R) \sim -1/R$.

In the second case, the form appropriate for the analysis of the large-R behaviour can be obtained by the Poisson summation formula

$$P_T(R) = \frac{4}{\sqrt{\pi D_0}} \sum_{m=1}^{\infty} (-1)^{m+1} m^2 \left\langle \exp \left(-\frac{m^2 R^2}{4 D_0 \int_0^T V(B_t) \mathrm{d}t} \right) \Big/ \sqrt{\int_0^T V(B_t) \mathrm{d}t} \right\rangle. \tag{47}$$

Further on, using the integral identity

$$\exp \left(-c^2 / (4b) \right) / \sqrt{b} = \frac{2}{\sqrt{\pi}} \int_0^{\infty} \exp \left(-b q^2 \right) \cos(cq) \, \mathrm{d}q, \tag{48}$$

we cast (47) into the form

$$P_T(R) = \frac{8}{\pi} \sum_{m=1}^{\infty} (-1)^{m+1} m^2 \int_0^{\infty} \cos(mRq) \Upsilon(T; q^2) \mathrm{d}q. \tag{49}$$

In case of standard Brownian motion the latter expression reduces to the series in the first line in (3). One observes that in the limit $R \to \infty$ the integral in the latter expression is dominated by the behaviour of $\Upsilon(T; q^2)$ in the vicinity of $q = 0$, which corresponds to the small-λ asymptotic behaviour of the moment-generating function in (8) (and hence, to such realisations of B_t for which $D_0 \int_0^T V(B_t) \mathrm{d}t$ is large). However, we find $1 - \Upsilon(T; q^2) = O(q^2)$ for models I and III (while for model II there are logarithmic corrections to the q^2-dependence), meaning that $P_T(R)$ decays sufficiently fast in all three models to ensure the existence of all moments. Hence, the precise form of the large-R tails of $P_T(R)$ cannot be, in principle, deduced from the small-q expansions of $\Upsilon(T; q^2)$ and we have to perform the corresponding integrals explicitly. In doing so, we will demonstrate below that the large-R tails of $P_T(R)$ are markedly different in all three models.

Relation (49) between $P_T(R)$ and the moment-generating function $\Upsilon(T; \lambda)$ of $D_0 \int_0^T V(B_t) \mathrm{d}t$ implies a simple and quite general relation between the moments of the range and the moments of the latter random variable. Indeed, multiplying both sides of (47) by R^q ($q \geqslant 0$) we find that whenever the moments of $D_0 \int_0^T V(B_t) \mathrm{d}t$ exist, the following relation holds

$$\begin{aligned}
\overline{\langle \mathcal{R}_T^q \rangle} &= \int_0^{\infty} R^q P_T(R) \mathrm{d}R \\
&= \frac{4(2^q - 4)}{\sqrt{\pi}} \Gamma\left(\frac{q+1}{2}\right) \zeta(q-1) \left\langle \left(D_0 \int_0^T V(B_t) \mathrm{d}t\right)^{q/2} \right\rangle,
\end{aligned} \tag{50}$$

where $\zeta(z)$ is the Riemann zeta function (note that for $q = 0, 1, 2$, one has to take the limit as q approaches one of these integer values). For instance, we find

$$\overline{\langle \mathcal{R}_T \rangle} = \frac{4}{\sqrt{\pi}} \left\langle \left(D_0 \int_0^T V(B_t) \mathrm{d}t\right)^{1/2} \right\rangle, \tag{51}$$

$$\overline{\langle \mathcal{R}_T^2 \rangle} = (8 \ln 2) \left\langle \left(D_0 \int_0^T V(B_t) \mathrm{d}t\right) \right\rangle, \tag{52}$$

and so on. Next, resorting again to the usual 'replica trick' we also deduce from (50) a linear relation between the averaged logarithm of the range and the averaged logarithm of $D_0 \int_0^T V(B_t) \mathrm{d}t$, which thus connects the 'typical' behaviour of these two random variables,

$$\begin{aligned}
\overline{\langle \ln \mathcal{R}_T \rangle} &= \lim_{q \to 0} \frac{1}{q} \left(\overline{\langle \mathcal{R}_T^q \rangle} - 1\right) \\
&= \frac{1}{2} \left\langle \ln\left(D_0 \int_0^T V(B_t) \mathrm{d}t\right) \right\rangle - 1 - \gamma/2 - \frac{4}{3} \ln 2 + 12 \ln A \\
&\approx \frac{1}{2} \left\langle \ln\left(D_0 \int_0^T V(B_t) \mathrm{d}t\right) \right\rangle + 0.7723.
\end{aligned} \tag{53}$$

In (53) $A \approx 1.2824$ is Glaisher's constant—a mathematical constant related to the asymptotical behaviour of the Barnes G-function (double gamma-function) [80]. The latter emerges, e.g. in the normalisation of the joint distributions of eigenvalues in Gaussian ensembles of the random matrix theory and, hence, A plays an important role in the asymptotic analysis of some characteristic properties of such ensembles (see, e.g. [81]).

We emphasise that (50) and (53) are general formulae which are valid for any positive functional $V(B_t)$ of Brownian motion B_t. In particular, they also hold in the trivial case when $V(B_t) \equiv 1$, i.e. when $\mathcal{R}_T = \mathcal{R}_T^{(\mathrm{BM})}$, the range of standard Brownian motion. For this latter case expression (53) yields the following result for the typical range $R_{\mathrm{typ}}^{(\mathrm{BM})}$ of standard Brownian motion,

$$R_{\mathrm{typ}}^{(\mathrm{BM})} = a \exp\left(\overline{\ln\left(\mathcal{R}_T^{(\mathrm{BM})}/a\right)}\right) = \frac{A^{12}}{2^{4/3} \exp(1 + \gamma/2)} \sqrt{D_0 T} \approx 2.1647 \sqrt{D_0 T} \tag{54}$$

where a is an auxiliary length scale which was introduced in order to get dimensionless units. While the scaling of the typical range with $\sqrt{D_0 T}$ appears quite intuitive, the proportionality factor ≈ 2.1647 in (54)

is rather nontrivial. In particular, its relation to the Glaisher's constant A is surprizing. Note that the expected value of the range in (51) also scales as $\sqrt{D_0 T}$, but the proportionality factor $4/\sqrt{\pi} \approx 2.2568$ is somewhat larger. As a consequence, for most of realisations of trajectories of standard Brownian motion their ranges appear to be smaller than the range averaged over all realisations, which implies that some less probable, atypical realisations dominate the value of the range. This, in turn, implies that even in the case of simple standard Brownian motion the knowledge of the full probability density function of the range is vital.

We now evaluate explicit expressions for $P_T(R)$ for the three models of random diffusivity presented in section 2 and discuss their asymptotic behaviour.

4.1. Model I

In model I we have $V(B_t) = \Theta(B_t)$ and, hence, the exponential function of $\int_0^T \Theta(B_t) dt$ in (46) is simply the moment-generating function of the occupation time of Brownian motion on a positive half-axis in the time interval $(0, T)$. Explicitly one has (see [53] for more details)

$$\Upsilon(T; \lambda) = \exp\left(-\lambda D_0 T/2\right) I_0\left(\lambda D_0 T/2\right),\tag{55}$$

such that

$$\Psi_T^{(I)}(R) = \frac{8}{\pi^2} \sum_{m=0}^{\infty} \frac{1}{(2m+1)^2} \exp\left(-\frac{\pi^2(2m+1)^2 D_0 T}{2R^2}\right) I_0\left(\frac{\pi^2(2m+1)^2 D_0 T}{2R^2}\right).\tag{56}$$

The latter expression together with (45) yields our result (12).

The small-R behaviour of $\Psi_T^{(I)}(R)$ and, hence, of the probability density function $P_T^{(I)}(R)$ can be derived directly from (56) by taking advantage of the asymptotic expansion

$$\exp\left(-x\right) I_0(x) \simeq \frac{1}{\sqrt{2\pi^3 x}} \sum_{k=0}^{\infty} \frac{\Gamma^2(k+1/2)}{k!(2x)^k},\tag{57}$$

which holds for large values of the argument x. Inserting this expansion into (56) and performing the summation over m we find

$$\Psi_T^{(I)}(R) \simeq \frac{8R}{\pi^{9/2}\sqrt{D_0 T}} \sum_{k=0}^{\infty} \left(1 - 2^{-3-2k}\right) \frac{\zeta(3+2k)\Gamma^2(k+1/2)}{k!} \left(\frac{R^2}{\pi^2 D_0 T}\right)^k.\tag{58}$$

By virtue of expression (45) the asymptotic small-R expansion for $P_T^{(I)}(R)$ is obtained from (58) by merely multiplying the latter by R and differentiating the resulting expression twice with respect to R. In doing so we arrive at a rather curious conclusion that, in contrast to the behaviour of the probability density function of the range of standard Brownian motion, $P_T^{(I)}(R)$ does not vanish in the limit $R \to 0$ but rather approaches the non-trivial constant value

$$P_T^{(I)}(R) \simeq \frac{14\zeta(3)}{\pi^{7/2}\sqrt{D_0 T}} \quad (R \to 0).\tag{59}$$

Therefore, despite the fact that the process x_t in model I exhibits the 'diffusive' behaviour $\langle x_t^2 \rangle = D_0 t$, its rather intricate character causes significant departures from the behaviour of standard Brownian motion—here, the fact that x_t may pause at the origin for a random time (having a broad distribution without even the first moment) once B_t goes initially to negative values, entails a finite value of the probability density at $R = 0$. This behaviour is also in line with the divergence of $P_T^{(I)}(M)$ in the limit $M \to 0$. Note that in (59) the amplitude decays as the inverse square root of T.

To construct the asymptotic large-R expansion of $P_T^{(I)}(R)$ we turn to the representation in (49). Using (55) we then have

$$\int_0^{\infty} \cos(mRq)\, e^{-D_0 T q^2/2} I_0\left(\frac{D_0 T}{2} q^2\right) dq = \frac{1}{\sqrt{4\pi D_0 T}} \exp\left(-\frac{m^2 R^2}{8 D_0 T}\right) K_0\left(\frac{m^2 R^2}{8 D_0 T}\right),\tag{60}$$

and, hence, $P_T^{(I)}(R)$ is cast into the form in (13). The leading, large-R behaviour is provided by the first term in the series in the latter equation,

$$P_T^{(I)}(R) \simeq \frac{8}{\pi R} \exp\left(-\frac{R^2}{4 D_0 T}\right) \quad (R \to \infty),\tag{61}$$

i.e. the right tail of the distribution $P_T^{(I)}(R)$ vanishes faster than a Gaussian function due to the additional factor $1/R$.

4.2. Model II

In model II the dimensionless diffusivity is governed by geometric Brownian motion: $V(B_t) = \exp(-B_t/a)$. In this case, one has (see [82] and also [83, 84])

$$\Upsilon(T; \lambda) = \frac{2}{\pi} \int_0^\infty \exp\left(-\frac{D_B T z^2}{4a^2}\right) \cosh\left(\frac{\pi z}{2}\right) K_{iz}\left(2a\sqrt{\lambda D_0/D_B}\right) \mathrm{d}z. \tag{62}$$

Combining (62), (45) and (46), we thus arrive at our result (15). The small-R asymptotic behaviour of $\Psi_T^{(II)}(R)$ and, hence, of $P_T^{(II)}(R)$ (see (15)) can be conveniently accessed by taking advantage of the Kontorovich–Lebedev-type representation in (62). Using the large-x expansion

$$K_{iz}(x) = \sqrt{\frac{\pi}{2x}} \exp(-x) \left(1 - \frac{1 + 4z^2}{8x} + \frac{(1 + 4z^2)(9 + z^2)}{2!(8x)^2} + O\left(\frac{1}{x^3}\right)\right), \tag{63}$$

we find from (46) that $\Psi_T^{(II)}(R)$ (see (15)) admits the following form in the limit $R \to 0$,

$$\Psi_T^{(II)}(R) = \frac{8}{\pi^2} \left(\frac{2aR}{\pi\sqrt{D_0 D_B}T}\right)^{1/2} \exp\left(\frac{\pi^2 a^2}{4D_B T}\right) \sum_{m=0}^\infty \frac{1}{(2m+1)^{5/2}}$$

$$\times \exp\left(-\frac{2\pi(2m+1)a}{R}\sqrt{\frac{D_0}{D_B}}\right) \left[1 - \frac{\tau^2 + 8\tau + 4\pi^2}{8\tau^2} \frac{R}{2\pi(2m+1)a}\sqrt{\frac{D_B}{D_0}}\right.$$

$$+ \frac{9\tau^4 + 80\tau^3 + 192\tau^2 + 40\pi^2\tau^2 + 192\pi^2\tau + 16\pi^4}{128\tau^4} \left(\frac{R}{2\pi(2m+1)a}\sqrt{\frac{D_B}{D_0}}\right)^2$$

$$\left. + O\left(\frac{R^3}{(2m+1)^3}\right)\right], \quad \tau = \frac{D_B T}{a^2}. \tag{64}$$

We notice next that the leading in the $R \to 0$ behaviour is provided by the term with $m = 0$. As a consequence, we arrive at the asymptotic formula

$$P_T^{(II)}(R) \simeq 32 \left(\frac{4D_0^3}{\pi^2 D_B^5 T^2}\right)^{1/4} \left(\frac{a}{R}\right)^{5/2} \exp\left(\frac{\pi^2 a^2}{4D_B T} - \sqrt{\frac{D_0}{D_B}}\frac{2\pi a}{R}\right) \quad (R \to 0). \tag{65}$$

Therefore, in model II the probability density function vanishes as $R \to 0$, in contrast to model I. Note also that the essential singularity in model II is somewhat weaker, $\ln P_T^{(II)}(R) \propto 1/R$, as compared to the singular behaviour specific to standard Brownian motion, for which one has $\ln P_T^{(BM)}(R) \propto 1/R^2$, see (3).

The analysis of the large-R asymptotic behaviour of $P_T^{(II)}(R)$ hinges on the expansion (49). Inserting (62) into (49) and evaluating the two-fold integral

$$\frac{2}{\pi} \int_0^\infty \exp\left(-\frac{D_B T}{4a^2}z^2\right) \cosh\left(\frac{\pi z}{2}\right) \int_0^\infty \cos(mRx)K_{iz}\left(2a\sqrt{\frac{D_0}{D_B}}x\right) \mathrm{d}x\,\mathrm{d}z$$

$$= \frac{\sqrt{\pi}a}{\sqrt{(D_B m^2 R^2 + 4a^2 D_0)\,T}} \exp\left(-\frac{a^2}{D_B T}\operatorname{arcsinh}^2\left(\sqrt{\frac{D_B}{D_0}}\frac{mR}{2a}\right)\right), \tag{66}$$

we find that expression (49) for model II admits the explicit form in (16). Inspecting the latter formula we notice that the dominant large-R behaviour is provided by the term with $m = 1$. As a consequence, we get

$$P_T^{(II)}(R) \simeq \frac{8a}{\sqrt{\pi D_B T}\,R} \exp\left(-\frac{a^2}{D_B T}\ln^2\left(\sqrt{\frac{D_B}{D_0}}\frac{R}{a}\right)\right) \quad (R \to \infty), \tag{67}$$

whose form is nearly identical (apart from numerical factors) to the asymptotic result (30) describing the right tail of the probability density function $P_T^{(II)}(M)$.

4.3. Model III

In model III the random diffusivity is given by $V(B_t) = B_t^2/a^2$ and the moment-generating function is (see [53, 85, 86])

$$\Upsilon(T; \lambda) = \frac{1}{\sqrt{\cosh(cT\sqrt{\lambda})}}, \quad c = 2\sqrt{D_B D_0/a^2}, \tag{68}$$

Hence, we find that

$$\Psi_T^{(\mathrm{III})}(R) = \frac{8}{\pi^2} \sum_{m=0}^{\infty} \frac{1}{(2m+1)^2} \frac{1}{\cosh^{1/2}\left(2\pi(2m+1)\frac{\sqrt{D_0 D_B T}}{aR}\right)}. \tag{69}$$

The latter expression, together with (45) and (46), result in (18). The small-R asymptotic behaviour of $P_T^{(\mathrm{III})}(R)$ can be obtained directly from (69) by noticing that the series converges very rapidly and the dominant behaviour is provided by the zeroth term, i.e.

$$\Psi_T^{(\mathrm{III})}(R) \simeq \frac{8\sqrt{2}}{\pi^2} \exp\left(-\frac{\pi\sqrt{D_0 D_B}\, T}{aR}\right). \tag{70}$$

Substituting the latter asymptotic form into (45) and differentiating, we arrive at

$$P_T^{(\mathrm{III})}(R) \simeq \frac{8\sqrt{2} D_0 D_B T^2}{a^2 R^3} \exp\left(-\frac{\pi\sqrt{D_0 D_B}\, T}{aR}\right) \quad (R \to 0), \tag{71}$$

which shows that $P_T^{(\mathrm{III})}(R)$ vanishes exponentially fast when $R \to 0$.

The large-R asymptotic behaviour of the probability density function of the range in model III can be determined as follows. Using again relation (68) we get

$$\int_0^{\infty} \cos(mRq)\Upsilon(T; q^2)\mathrm{d}q = \frac{1}{2c\sqrt{2\pi}\,T}\left|\Gamma\left(\frac{1}{4} + \mathrm{i}\frac{mR}{2cT}\right)\right|^2, \tag{72}$$

which yields our result (19). Noticing finally that in the limit $R \to \infty$ the dominant contribution to the expansion in (19) comes from the term $m = 1$ we thus arrive at the asymptotic formula

$$P_T^{(\mathrm{III})}(R) \simeq \frac{4\sqrt{2}}{\sqrt{\pi}(D_0 D_B T^2)^{1/4}} \sqrt{\frac{a}{R}} \exp\left(-\frac{\pi aR}{4\sqrt{D_0 D_B}\, T}\right) \quad (R \to \infty). \tag{73}$$

Figure 4 illustrates the behaviour of the probability density function $P_T(R)$ and its asymptotic forms for the three models. To emphasise the crossover behaviours as well as the asymptotic forms of the probability density functions we show the results both on linear and log–log scales. Note specifically that while models II and III exhibit a suppression of the probability density functions to zero in the limit $R \to 0$, in model I a finite value at $R = 0$ is reached.

In figure 5 we compare the probability density functions $P_T(M)$ and $P_T(R)$ for the three random diffusivity models. Note the different large-M asymptotic behaviours for the different models as discussed above. The analytical results are also confronted with Monte Carlo simulations. These simulations were obtained with the Euler integration scheme applied to the Langevin equation (4). For each realisation an independent Brownian motion run is generated to compute the dimensionless random diffusivity through the specific functional $V(B_t)$. In this way the two noises are varied simultaneously and independently. Perfect agreement with analytical formulas is observed even for a moderately large sampling with 10 000 realisations.

4.4. Relation between the moments of the maximum and of the range

We derive a general expression for the moments of the range for the processes in (4). To this end, we observe that for the three models studied here the probability density function $P_T(R)$ can be formally written as

$$P_T(R) = 4\sum_{m=1}^{\infty} (-1)^{m+1} m^2 P_T(M = mR), \tag{74}$$

where $P_T(M)$ is the corresponding probability density function of the maximum. One may expect that this relation is valid in general for an arbitrary process defined in (4) but we are not in the position to prove it here. Then, multiplying both sides of the latter expression by R^q we obtain, through a simple change of the integration variable, the following intricate relation between the moments of the range and the moments of the maximum,

$$\overline{\langle \mathcal{R}_T^q \rangle} = 4\left(1 - 2^{2-q}\right)\zeta(q-1)\overline{\langle \mathcal{M}_T^q \rangle}. \tag{75}$$

In particular, we get

$$\overline{\langle \mathcal{R}_T \rangle} = 2\overline{\langle \mathcal{M}_T \rangle} \tag{76}$$

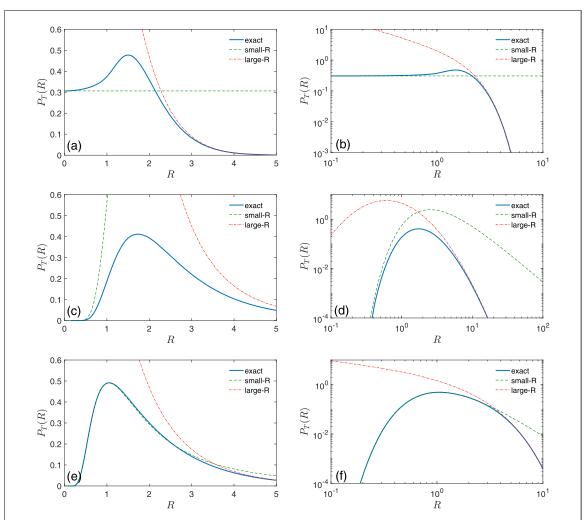$$\overline{\langle \mathcal{R}_T^2 \rangle} = 4\ln(2)\overline{\langle \mathcal{M}_T^2 \rangle}, \tag{77}$$

Figure 4. Probability density function $P_T(R)$ of the range and its small-R and large-R asymptotic behaviours, for model I (a) and (b), model II (c) and (d), and model III (e) and (f), plotted on linear (a), (c), (e) and log–log (b), (d) and (f) scales. We set $D_0 = 1$, $T = 1$, $a = 1$, and $D_B = 1$. Compare this behaviour to the Brownian limit in figure 1.
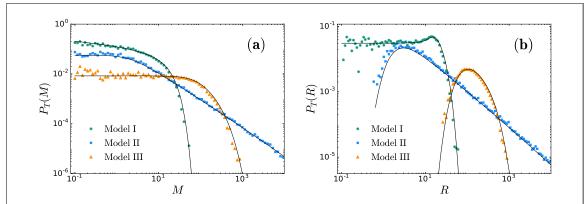

Figure 5. Comparison of the probability density functions $P_T(M)$ (a) and $P_T(R)$ (b) for the three random diffusivity models. Solid lines show the analytical formulas whereas symbols represent the empirically renormalised histograms obtained from Monte Carlo simulations with 10^4 runs (time step 10^{-2}). We set $D_0 = 1$, $T = 100$, $a = 1$, and $D_B = 1$.

$$\overline{\langle \mathcal{R}_T^3 \rangle} = \frac{\pi^2}{3} \overline{\langle \mathcal{M}_T^3 \rangle}, \tag{78}$$

and so on. While the first relation (76) is obvious, relations (77) and (78) are non-trivial results. Lastly, comparing (76) and (50), we arrive at (42), which we presented without a derivation in the previous section.

As a direct consequence of relation (75) we can write down exact closed-form expressions for the moments of the range of arbitrary (not necessarily integer) order. In turn, the latter permit us to evaluate

the coefficients of variation of the distributions of the range. For model I we find

$$v_R^{(\mathrm{I})} = \sqrt{\frac{\pi^3 \ln(2) - 16}{16}} \approx 0.586, \tag{79}$$

which is about 30 per cent smaller than the coefficient of variation (27) of the corresponding distribution of the maximum. The coefficient of variation of the range for model II is given explicitly by

$$v_R^{(\mathrm{II})} = \sqrt{\ln(2)} \frac{\sqrt{1 - 2 \exp\left(-\tau/2\right) \, \mathrm{erf}^2(\sqrt{\tau}/2)/\ln(2) - \exp(-\tau)}}{\sqrt{2} \, \mathrm{erf}(\sqrt{\tau}/2)} \exp\left(\tau/4\right), \tag{80}$$

and, hence, grows as $\sqrt{\ln(2)/2} \exp(\tau/4)$ in the limit $\tau \to \infty$. This growth is thus somewhat slower than for the corresponding coefficient of variation (33) of the distribution of the maximum due to the additional numerical factor $\sqrt{\ln(2)} \approx 0.833$. Lastly, for model III the numerical value of the coefficient of variation of $P_T^{(\mathrm{III})}(R)$ is

$$v_R^{(\mathrm{III})} \approx 0.635, \tag{81}$$

i.e. is again somewhat smaller than the corresponding value $v_M^{(\mathrm{III})}$ for the maximum, equation (41). We thus conclude that distributions of the range in all three models under study are *narrower* than the corresponding probability density functions of the maxima.

5. Typical behaviour of the probability density function of the maximum

As yet, our discussion of the averaged versus a typical behaviour concerned only the maximum and the range themselves. The results for $P_T(M)$ and $P_T(R)$ we have presented so far correspond to a standard way of performing the averaging, i.e. when the averaging is first performed with respect to thermal histories at a fixed realisation of the stochastic diffusivity process B_t and then over all possible realisations of B_t. Conversely, realisation-dependent distributions $\mathcal{P}_T(M)$ and $\mathcal{P}_T(R)$ are evidently random functions themselves which fluctuate from one realisation of B_t to the next, and it is, of course, not clear *a priori* to which extent their first moments, i.e. precisely $P_T(M)$ and $P_T(R)$, are representative of the actual behaviour of these properties. In principle, it may well happen that $P_T(M)$ and $P_T(R)$ are supported by some atypical, rare realisations of B_t which nonetheless provide a dominant contribution to their values. If true, in order to observe our predictions for $P_T(M)$ and $P_T(R)$ one may need very large statistical samples. Note that in figure 5 we presented a convincing evidence for the predicted functional forms but the number of realisations used to perform the averaging was sufficiently high, 10^4. That may not be the case for experimental studies for which such a large number is beyond reach.

Following the analysis of a typical kinetic behaviour in the so-called target problem with respect to fluctuations in the starting points of searchers (see reference [74] and the recent reference [75]), we concentrate on the properties defined in (9). Here, one first performs an averaging over thermal histories at a fixed realisation of B_t and then averages the *logarithm* of the realisation-dependent probability density over all possible realisations of B_t. Because the logarithm is a slowly-varying function of its argument, one expects that its averaged behaviour is rather insensitive to rare anomalous realisations and is thus representative of a typical behaviour which should be observed for a majority of trajectories B_t, or seen for small statistical samples. The resulting expression is then exponentiated to produce an estimate of typical distributions. We will be concerned here only with the typical behaviour of the distribution of the maximum—the analysis of the typical distribution of the range appears to be somewhat more involved and lengthy, but we do not expect any significant new features, as compared to the behaviour of the maximum.

Recalling that for any given realisation of B_t, the probability density function $\mathcal{P}_T(M)$ is given by (2) with $D_0 T$ replaced by $D_0 \int_0^T V(B_t)\mathrm{d}t$, we then have that

$$\langle \ln(\mathcal{P}_T(M)/p) \rangle = -\frac{1}{2} \left\langle \ln\left(\pi p^2 D_0 \int_0^T V(B_t)\mathrm{d}t\right)\right\rangle - \left\langle \frac{1}{D_0 \int_0^T V(B_t)\mathrm{d}t}\right\rangle \frac{M^2}{4} \tag{82}$$

and hence,

$$P_T^{(\mathrm{typ})}(M) = p\frac{\mathcal{N}_M}{\sqrt{\pi}} \exp\left(-\frac{1}{2}\left\langle \ln\left(p^2 D_0 \int_0^T V(B_t)\mathrm{d}t\right)\right\rangle\right.$$
$$\left. - \left\langle \frac{1}{D_0 \int_0^T V(B_t)\mathrm{d}t}\right\rangle \frac{M^2}{4}\right). \tag{83}$$
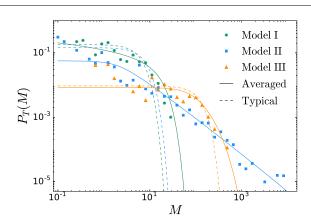
Figure 6. Comparison of the probability density functions $P_T(M)$ (solid curves) and the estimate $P_T^{(\text{typ})}(M)$ from (85) of the typical behaviour (dashed curves) for the three random diffusivity models. Symbols represent the empirically renormalised histograms obtained from Monte Carlo simulations with 10^2 runs (the time step of 10^{-2}). We set $D_0 = 1$, $T = 100$, $a = 1$, and $D_B = 1$.

Integrating the latter expression over M we find that the normalisation is given by

$$\mathcal{N}_M = \left\langle \frac{1}{D_0 \int_0^T V(B_t)\mathrm{d}t} \right\rangle^{1/2} \exp\left(\frac{1}{2} \left\langle \ln\left(p^2 D_0 \int_0^T V(B_t)\mathrm{d}t \right) \right\rangle \right) \tag{84}$$

such that, eventually, we have the following estimate of the typical behaviour

$$P_T^{(\text{typ})}(M) = \frac{1}{\sqrt{\pi}} \left\langle \frac{1}{D_0 \int_0^T V(B_t)\mathrm{d}t} \right\rangle^{1/2} \exp\left(-\left\langle \frac{1}{D_0 \int_0^T V(B_t)\mathrm{d}t} \right\rangle \frac{M^2}{4} \right). \tag{85}$$

Therefore, we arrive at the conclusion that if the first inverse moment of the random variable $D_0 \int_0^T V(B_t)\mathrm{d}t$ exists, the distribution $P_T^{(\text{typ})}(M)$ is a Gaussian function, similar to the case of a standard Brownian motion, (2), with a variance that is reciprocal to the negative moment of $D_0 \int_0^T V(B_t)\mathrm{d}t$. Both results become identical, of course, when $V(B_t) = 1$.

The first inverse moment of $D_0 \int_0^T V(B_t)\mathrm{d}t$ can be calculated straightforwardly by simply integrating $\Upsilon(T; \lambda)$ in (8) over λ from zero to infinity. In doing so, we realise that for model I this negative moment does not exist, because $\Upsilon(T; \lambda)$ decays as $1/\sqrt{\lambda}$ in the limit $\lambda \to \infty$ (see (55)) and hence, the integral diverges at the upper integration limit. On the other hand, the average of $1/(D_0 \int_0^T V(B_t)\mathrm{d}t)$ over any *finite* statistical sample of trajectories B_t is evidently finite and hence, in virtue of (85) for such samples $P_T^{(\text{typ})}(M)$ should have a Gaussian shape. In figure 6 we compare the ensemble-averaged $P_T^{(\text{I})}(M)$ (equation (11), solid curve) and $P_T^{(\text{typ})}(M)$ (equation (85), dashed curve) against an empirical histogram obtained from Monte Carlo simulations with 100 realisations of trajectories B_t only, i.e. for a statistical sample which is 100 times less than the one used to produce figure 5. Note that here $\langle 1/(D_0 \int_0^T V(B_t)\mathrm{d}t) \rangle$ is evaluated numerically by averaging over this finite set of realisations. We observe that for sufficiently small values of M, (i.e. those close to the most probable value of M), for such a moderately small sample the estimate $P_T^{(\text{typ})}(M)$ indeed agrees with the numerically evaluated distribution better than $P_T^{(\text{I})}(M)$. For larger values of M, however, the Gaussian tail of $P_T^{(\text{I})}(M)$ seems to be closer to the numerical curve than that of $P_T^{(\text{typ})}(M)$ even for such a small sample. Upon an increase of the number of realisations of B_t, we get progressively bigger values of $\langle 1/(D_0 \int_0^T V(B_t)\mathrm{d}t) \rangle$ and therefore the variance in the Gaussian function in (85) vanishes meaning that $P_T^{(\text{typ})}(M)$ converges to the delta-function, while the Gaussian tail of $P_T^{(\text{I})}(M)$ is characterised by a finite variance. This implies that for progressively larger statistical samples $P_T^{(\text{typ})}(M)$ may describe correctly the shape of the numerically evaluated distribution only in a close vicinity of $M = 0$, while for the almost entire range of variation of M the ensemble-averaged distribution $P_T^{(\text{I})}(M)$ should provide an accurate estimate of the actual behaviour (see figure 5).

The first inverse moment of $D_0 \int_0^T V(B_t)\mathrm{d}t$ is finite for both models II and III. For model II we have

$$\left\langle \frac{1}{D_0 \int_0^T V(B_t)\mathrm{d}t} \right\rangle = \frac{D_B}{2a^2 D_0} \int_0^\infty z \, \mathrm{d}z \, \coth\left(\frac{\pi z}{2} \right) \exp\left(-\frac{D_B T}{4a^2} z^2 \right), \tag{86}$$

where the integral in the right-hand side is finite for any finite value of the parameter $D_B T / 4a^2$. The latter integral cannot be performed exactly but its behaviour can be readily understood by noticing that for any $z \geqslant 0$ we have

$$\frac{2}{\pi} \leqslant z \coth\left(\frac{\pi z}{2}\right) \leqslant z + \frac{2}{\pi}. \tag{87}$$

As a consequence, we find that the first inverse moment of $D_0 \int_0^T V(B_t) \mathrm{d}t$ obeys the following two-sided inequality

$$\frac{1}{aD_0}\sqrt{\frac{D_B}{\pi T}} \leqslant \left\langle \frac{1}{D_0 \int_0^T V(B_t)\mathrm{d}t} \right\rangle \leqslant \frac{1}{aD_0}\sqrt{\frac{D_B}{\pi T}}\left(1 + a\sqrt{\frac{\pi}{D_B T}}\right). \tag{88}$$

In the limit $T \to \infty$ these bounds become sharp and hence, define the leading behaviour of the first inverse moment exactly.

For model III the first inverse moment of $D_0 \int_0^T V(B_t)\mathrm{d}t$ has the simpler form

$$\left\langle \frac{1}{D_0 \int_0^T V(B_t)\mathrm{d}t} \right\rangle = \frac{c_1 a^2}{2D_0 D_B T^2}, \quad c_1 = \int_0^\infty \frac{z\,\mathrm{d}z}{\sqrt{\cosh(z)}} \approx 5.563. \tag{89}$$

Comparison of our analytical predictions for the ensemble-averaged and the typical behaviours for models II and III against the histograms obtained from Monte Carlo simulations with just 100 realisations of the stochastic process B_t is presented in figure 6. Here, for $P_T^{(\mathrm{typ})}(M)$ we used our result in (85) with the respective variance given by our analytical expressions in (86) (model II) and (89) (model III). We observe that for model II for small values of M again $P_T^{(\mathrm{typ})}(M)$ provides a better estimate of the actual behaviour than $P_T^{(\mathrm{II})}(M)$—the former predicts higher values of the probabilities while the latter underestimates them: a trend that is confirmed by our numerical observations. This is not the case for larger values of M. Perhaps somewhat surprisingly, the heavy log-normal tail of $P_T^{(\mathrm{II})}(M)$ appears in a good agreement with numerics even for such a moderately small sample size for values of M as large as 10^3. In turn, for model III there is no significant difference between $P_T^{(\mathrm{typ})}(M)$ and $P_T^{(\mathrm{III})}(M)$ for small values of M, a circumstance that does not permit to make any conclusive statement. On the contrary, in the large-M domain, the ensemble-average result $P_T^{(\mathrm{III})}(M)$ seems to be more accurate.

6. Conclusion

Deviations from standard Brownian motion have been measured in a vast range of systems, starting with Richardson's cubic law for the relative diffusion of tracers in turbulent media in 1926 [87]. Such 'anomalous diffusion' has given rise to a rich variety of statistical models accounting for various physical aspects effecting deviations from standard Brownian motion [88–90]. As a particular case, random diffusivity models were introduced in the context of the modelling of complex measured NMR signals [91]. The randomness of the diffusivity can be assumed to be due to an inhomogeneous particle ensemble in a homogeneous environment, or due to identical particles in a heterogeneous environment. When the diffusivity distribution is fixed in time the dynamics resulting from such random diffusivities is captured by the framework of superstatistics [92] or grey Brownian motion [93]. When particles move in quenched environments with finite patch sizes and specific jump rules interesting dynamic effects and non-Gaussian phenomena have recently been revealed [94, 95].

Originally devised to reproduce the observed crossover behaviour from non-Gaussian to Gaussian displacement statistics in systems showing a Brownian scaling of the mean squared displacement [96, 97], diffusive processes with *stochastically evolving* diffusivities were devised as an 'annealed' approach to the motion of the test particle in a heterogeneous environment. Such diffusing diffusivity models with stationary diffusivity dynamics were analysed in terms of the mean squared displacement and the displacement distribution. Despite the different formulations several core features turn out to be robust among these models [54, 55, 57–59, 98].

Here we studied a stochastic process x_t driven by white Gaussian noise, whose amplitude is being modulated by a stochastically varying diffusivity D_t for three different choices: (I) cut-off Brownian motion B_t with $D_t \sim \Theta(B_t)$; (II) geometric Brownian motion, $D_t \sim \exp(-B_t)$; and (III) squared Brownian motion, $D_t \sim B_t^2$. In contrast to the above-mentioned diffusing diffusivity models, that are all Brownian, the three choices here effect non-stationary diffusivity dynamics, and the resulting diffusion exhibits both normal and anomalous diffusive scaling.

In the analysis we concentrated on the extremal properties in terms of the maximum and the range of these three random diffusivity models. We obtain analytical expressions for the probability density functions of the maximum and the range of the processes for a given observation time. Our discussion

reveals both similarities and differences of the extremal properties of these models among each other as well as compared to standard Brownian motion. In particular, we unveil that model I shows significant differences from Brownian motion while the small-maximum limit of model II coincides exactly with the Brownian behaviour. We also show that the distributions of the maximum are generically broader than the distributions of the range, as evidenced by the analysis of the coefficients of variation of the corresponding distributions. Our discussion finally unveils the difference between the ensemble and the typical behaviour of the probability density functions, an important ingredient for the analysis of finite-sized data sets.

The analysis of given stochastic time series representing a set of trajectories of diffusing test particles has more recently received considerable attention. A number of statistical observables has been introduced and discussed (see, e.g. [89, 90, 99, 100]) to allow the physical classification of recorded data. For instance, it has been shown how to use Bayesian maximum likelihood [101, 102] or machine learning [103, 104] to classify a measured system and extract its physical parameters. Specifically, the power spectral analysis of single, finite-length trajectories was shown to distinguish different forms of random diffusivity models [53]. A more recent twist on data analysis of stochastic processes uses large-deviation approaches, for instance, for the time averaged mean squared displacement [105, 106].

While it is not surprising that the EV behaviour encoded in the probability density functions of the maximum and the range studied here was shown to distinguish the three, quite different, random diffusivity models investigated here, we also demonstrated that the rectified Brownian motion of model I exhibits significant differences to standard Brownian motion. It should therefore be interesting to investigate whether these two distributions allow one to distinguish between the diffusing diffusivity models encoding Brownian yet non-Gaussian motion [54, 55, 57–59], and how these measures change for projections of higher dimensional versions of these models.

Acknowledgments

ORCID iDs

Denis S Grebenkov ⬥ https://orcid.org/0000-0002-6273-9164
Vittoria Sposini ⬥ https://orcid.org/0000-0003-0915-4746
Ralf Metzler ⬥ https://orcid.org/0000-0002-6013-7020
Gleb Oshanin ⬥ https://orcid.org/0000-0001-8467-3226

References

[1] Lévy P 1948 *Processus Stochastiques et Mouvement Brownien* (Paris: Gauthier-Villars)
[2] Feller W 1951 The asymptotic distribution of the range of sums of independent random variables *Ann. Math. Stat.* **22** 427
[3] Borodin A N and Salminen P 1996 *Handbook of Brownian Motion: Facts and Formulae* (Basel: Birkhäuser)
[4] Lindenberg K and West B J 1981 The first, the biggest, and other such considerations *J. Stat. Phys.* **42** 201
[5] Redner S 2001 *A Guide to First-Passage Processes* (Cambridge: Cambridge University Press)
[6] Condamin S, Bénichou O, Tejedor V, Voituriez R and Klafter J 2007 First-passage times in complex scale-invariant media *Nature* **450** 77
[7] Schehr G and Le Doussal P 2010 Extreme value statistics from the real space renormalization group: Brownian motion, Bessel processes and continuous time random walks *J. Stat. Mech.* P01009
[8] Bénichou O and Voituriez R 2014 From first-passage times of random walks in confinement to geometry-controlled kinetics *Phys. Rep.* **539** 225
[9] Metzler R, Oshanin G and Redner S (ed) 2014 *First-Passage Phenomena and Their Applications* (Singapore: World Scientific)
[10] Bray A J, Majumdar S N and Schehr G 2013 Persistence and first-passage properties in nonequilibrium systems *Adv. Phys.* **62** 225
[11] Mejía-Monasterio C, Oshanin G and Schehr G 2011 First passages for a search by a swarm of independent random searchers *J. Stat. Mech.* P06022
[12] Mattos T, Mejía-Monasterio C, Metzler R and Oshanin G 2012 First passages in bounded domains: when is the mean first passage time meaningful? *Phys. Rev.* E **86** 031143
[13] Majumdar S N, Pal A and Schehr G 2020 Extreme value statistics of correlated random variables: a pedagogical review *Phys. Rep.* **840** 1

[14] Artime O, Khalil N, Toral R and San Miguel M 2018 First-passage distributions for the one-dimensional Fokker–Planck equation *Phys. Rev.* E **98** 042143

[15] Grebenkov D S 2020 Paradigm shift in diffusion-mediated surface phenomena *Phys. Rev. Lett.* **125** 078102

[16] Quinn G D, Bishop G H and Harrison R J 1976 On the cluster size distribution for critical percolation *J. Phys. A: Math. Gen.* **9** L9

[17] Redner S and Yang Z R 1982 Size and shape of directed lattice animals *J. Phys. A: Math. Gen.* **15** L177

[18] Chicheportiche R and Bouchaud J-P 2014 Some applications of first-passage ideas to finance *First-Passage Phenomena and Their Applications* ed R Metzler, G Oshanin and S Redner (Singapore: World Scientific) ch 18

[19] Wergen G, Bogner M and Krug J 2011 Record statistics for biased random walks, with an application to financial data *Phys. Rev.* E **83** 051109

[20] Mari J-F and Schott R 2001 *Probabilistic and Statistical Methods in Computer Science* (New York: Springer)

[21] Majumdar S N 2005 Brownian functionals in physics and computer science *Curr. Sci.* **89** 2076 https://jstor.org/stable/24111070

[22] Godrèche C, Majumdar S N and Schehr G 2017 Record statistics of a strongly correlated time series: random walks and Lévy flights *J. Phys. A: Math. Theor.* **50** 333001

[23] Majumdar S N, von Bomhard P and Krug J 2019 Exactly solvable record model for rainfall *Phys. Rev. Lett.* **122** 158702

[24] Fudenberg D and Tirole J 1991 *Game Theory* (Cambridge, MA: MIT Press)

[25] Finkelsetin M 2008 *Failure Rate Modelling for Reliability and Risk* (London: Springer)

[26] Eliazar I, Metzler R and Reuveni S 2019 Gumbel central limit theorem for max-min and min-max *Phys. Rev.* E **100** 020104(R)

[27] Eliazar I, Metzler R and Reuveni S 2019 Poisson-process limit-laws yield Gumbel max-min and min-max *Phys. Rev.* E **100** 022129

[28] Hughes B D 1996 *Random Walks and Random Environments* vol 1 (Oxford: Clarendon)

[29] Mori F, Majumdar S N and Schehr G 2019 Time between the maximum and the minimum of a stochastic process *Phys. Rev. Lett.* **123** 200201

[30] Mori F, Majumdar S N and Schehr G 2020 Distribution of the time between maximum and minimum of random walks *Phys. Rev.* E **101** 052111

[31] Collins F C and Kimball G E 1949 Diffusion-controlled reaction rates *J. Colloid Sci.* **4** 425

[32] von Hippel P H and Berg O 1989 Facilitated target location in biological systems *J. Biol. Chem.* **264** 675

[33] Godec A and Metzler R 2016 Universal proximity effect in target search kinetics in the few encounter limit *Phys. Rev.* X **6** 041037

[34] Grebenkov D, Metzler R and Oshanin G 2018 Strong defocusing of molecular reaction times results from an interplay of geometry and reaction control *Commun. Chem.* **1** 96

[35] Kolesov G, Wunderlich Z, Laikova O N, Gelfand M S and Mirny L A 2007 How gene order is influenced by the biophysics of transcription regulation *Proc. Natl Acad. Sci. USA* **104** 13948

[36] Pulkkinen O and Metzler R 2013 Distance matters: the impact of gene proximity in bacterial gene regulation *Phys. Rev. Lett.* **110** 198101

[37] Burlatsky S F, Oshanin G S, Mogutov A V and Moreau M 1992 Non-Fickian steady flux in a one-dimensional Sinai-type disordered system *Phys. Rev.* A **45** R6955

[38] Monthus C, Oshanin G, Comtet A and Burlatsky S F 1996 Sample-size dependence of the ground-state energy in a one-dimensional localization problem *Phys. Rev.* E **54** 231

[39] Yuste S B, Oshanin G, Lindenberg K, Bénichou O and Klafter J 2008 Survival probability of a particle in a sea of mobile traps: a tale of tails *Phys. Rev.* E **78** 021105

[40] Oshanin G, Rosso A and Schehr G 2012 Anomalous fluctuations of currents in Sinai-type random chains with strongly correlated disorder *Phys. Rev. Lett.* **110** 100602

[41] Dean D S, Gupta S, Oshanin G, Rosso A and Schehr G 2014 Diffusion in periodic, correlated random forcing landscapes *J. Phys. A: Math. Theor.* **47** 372001

[42] Dean D S, Iorio A, Marinari E and Oshanin G 2016 Sample-to-sample fluctuations of power spectrum of a random motion in a periodic Sinai model *Phys. Rev.* E **94** 032131

[43] Daniels H E and Smithies F 1941 The probability distribution of the extent of a random chain *Math. Proc. Camb. Phil. Soc.* **37** 244

[44] Weiss G H and Rubin R J 1983 Random walks: theory and selected applications *Adv. Chem. Phys.* **52** 363

[45] Berezhkovskii A M, Makhnovskii Y A and Suris R A 1989 Wiener sausage volume moments *J. Stat. Phys.* **57** 333

[46] Bénichou O, Krapivsky P L, Mejía-Monasterio C and Oshanin G 2016 Temporal correlations of the running maximum of a Brownian trajectory *Phys. Rev. Lett.* **117** 080601

[47] Bénichou O, Krapivsky P L, Mejía-Monasterio C and Oshanin G 2016 Joint distributions of partial and global maxima of a Brownian bridge *J. Phys. A: Math. Theor.* **49** 335002

[48] Deng P 2017 The joint distribution of running maximum of a Slepian process *Methodol. Comput. Appl. Probab.* **20** 1123

[49] Annesi B, Marinari E and Oshanin G 2019 Covariance of the running range of a Brownian trajectory *J. Phys. A: Math. Theor.* **52** 345003

[50] Wiese K J 2020 Span observables: 'when is a foraging rabbit no longer hungry?' *J. Stat. Phys.* **178** 625

[51] Grebenkov D S, Metzler R and Oshanin G 2019 Full distribution of first exit times in the narrow escape problem *New J. Phys.* **21** 122001

[52] Grebenkov D S, Metzler R and Oshanin G 2018 Towards a full quantitative description of single-molecule reaction kinetics in biological cells *Phys. Chem. Chem. Phys.* **20** 16393

[53] Sposini V, Grebenkov D S, Metzler R, Oshanin G and Seno F 2020 Universal spectral features of different classes of random-diffusivity processes *New J. Phys.* **22** 063056

[54] Chubynsky M V and Slater G W 2014 Diffusing diffusivity: a model for anomalous, yet Brownian, diffusion *Phys. Rev. Lett.* **113** 098302

[55] Jain R and Sebastian K L 2016 Diffusion in a crowded, rearranging environment *J. Phys. Chem.* B **120** 3988

[56] Cherstvy A G and Metzler R 2016 Anomalous diffusion in time-fluctuating non-stationary diffusivity landscapes *Phys. Chem. Chem. Phys.* **18** 23840

[57] Chechkin A V, Seno F, Metzler R and Sokolov I M 2017 Brownian yet non-Gaussian diffusion: from superstatistics to subordination of diffusing diffusivities *Phys. Rev.* X **7** 021002

[58] Tyagi N and Cherayil B J 2017 Non-Gaussian Brownian diffusion in dynamically disordered thermal environments *J. Phys. Chem.* B **121** 7204

[59] Lanoiselée Y and Grebenkov D S 2018 A model of non-Gaussian diffusion in heterogeneous media *J. Phys. A: Math. Theor.* **51** 145602

[60] Sposini V, Chechkin A V, Seno F, Pagnini G and Metzler R 2018 Random diffusivity from stochastic equations: comparison of two models for Brownian yet non-Gaussian diffusion *New J. Phys.* **20** 043044

[61] Lanoiselée Y and Grebenkov D S 2019 Non-Gaussian diffusion of mixed origins *J. Phys. A: Math. Theor.* **52** 304001

[62] Lanoiselée Y, Moutal N and Grebenkov D S 2018 Diffusion-limited reactions in dynamic heterogeneous media *Nat. Commun.* **9** 4398

[63] Sposini V, Chechkin A and Metzler R 2019 First passage statistics for diffusing diffusivity *J. Phys. A: Math. Theor.* **52** 04LT01

[64] Grebenkov D S 2019 A unifying approach to first-passage time distributions in diffusing diffusivity and switching diffusion models *J. Phys. A: Math. Theor.* **52** 174001

[65] Grebenkov D S, Sposini V, Metzler R, Oshanin G and Seno F 2021 Exact first-passage time distributions for three random diffusivity models *J. Phys. A: Math. Theor.* **54** 04LT01

[66] Baldovin F, Orlandini E and Seno F 2019 Polymerization induces non-Gaussian diffusion *Front. Phys.* **7** 124

[67] Hidalgo-Soria M and Barkai E 2020 Hitchhiker model for Laplace diffusion processes *Phys. Rev.* E **102** 012109

[68] Oshanin G and Moreau M 1995 Influence of transport limitations on the kinetics of homopolymerization reactions *J. Chem. Phys.* **102** 2977

[69] Heston S L 1993 A closed-form solution for options with stochastic volatility with applications to bond and currency options *Rev. Financ. Stud.* **6** 327

[70] Yamamoto E, Akimoto T, Mitsutake A and Metzler R 2020 Universal relation between instantaneous diffusivity and radius of gyration of proteins in aqueous solution (arXiv:2009.06829)

[71] Jeon J-H, Javanainen M, Martinez-Seara H, Metzler R and Vattulainen I 2016 Protein crowding in lipid bilayers gives rise to non-Gaussian anomalous lateral diffusion of phospholipids and proteins *Phys. Rev.* X **6** 021006

[72] Sabri A, Xu X, Krapf D and Weiss M 2020 Elucidating the origin of heterogeneous anomalous diffusion in the cytoplasm of mammalian cells *Phys. Rev. Lett.* **125** 058101

[73] Black F and Scholes M 1973 The pricing of options and corporate liabilities *J. Polit. Econ.* **81** 637

[74] Evans M R and Majumdar S N 2011 Diffusion with stochastic resetting *Phys. Rev. Lett.* **106** 160601

[75] Grebenkov D S, Metzler R and Oshanin G 2020 From single-particle stochastic kinetics to macroscopic reaction rates: fastest first-passage time of N random walkers *New J. Phys.* **22** 103004

[76] Castiglione P, Mazzino A, Muratore-Ginanneschi P and Vulpiani A 1999 On strong anomalous diffusion *Physica* D **134** 75

[77] Rebenshtok A, Denisov S, Hänggi P and Barkai E 2014 Non-normalizable densities in strong anomalous diffusion: beyond the central limit theorem *Phys. Rev. Lett.* **112** 110601

[78] Aghion E, Kessler D A and Barkai E 2017 Large fluctuations for spatial diffusion of cold atoms *Phys. Rev. Lett.* **118** 260601

[79] See https://oeis.org/A126156

[80] Askey R A and Roy R 2010 Barnes G-function *NIST Handbook of Mathematical Functions* ed F W J Olver, D M Lozier, R F Boisvert and C W Clark (Cambridge: Cambridge University Press)

[81] Vivo P, Pato M P and Oshanin G 2016 Random pure states: quantifying bipartite entanglement beyond the linear statistics *Phys. Rev.* E **93** 052106

[82] Oshanin G, Mogutov A and Moreau M 1993 Steady flux in a continuous-space Sinai chain *J. Stat. Phys.* **73** 379

[83] Monthus C c and Comtet A 1994 On the flux distribution in a one dimensional disordered system *J. Phys. I France* **4** 635

[84] Oshanin G and Schehr G 2012 Two stock options at the races: Black–Scholes forecasts *Quant. Finance* **12** 1325

[85] Cameron R H and Martin W T 1945 Transformations of Wiener integrals under a general class of linear transformation *Trans. Am. Math. Soc.* **58** 184
Cameron R H and Martin W T 1945 Evaluation of various Wiener integrals by use of certain Sturm–Liouville differential equations *Bull. Am. Math. Soc.* **51** 73

[86] Albers T and Radons G 2014 Weak ergodicity breaking and aging of chaotic transport in Hamiltonian systems *Phys. Rev. Lett.* **113** 184101

[87] Richardson L F 1926 Atmospheric diffusion shown on a distance-neighbour graph *Proc. R. Soc.* A **110** 709

[88] Bouchaud J-P and Georges A 1990 Anomalous diffusion in disordered media: statistical mechanisms, models and physical applications *Phys. Rep.* **195** 127

[89] Sokolov I M 2012 Models of anomalous diffusion in crowded environments *Soft Matter* **8** 9043

[90] Metzler R, Jeon J-H, Cherstvy A G and Barkai E 2014 Anomalous diffusion models and their properties: non-stationarity, non-ergodicity, and ageing at the centenary of single particle tracking *Phys. Chem. Chem. Phys.* **16** 24128

[91] Kärger J 1985 NMR self-diffusion studies in heterogeneous systems *Adv. Colloid Interface Sci.* **23** 129

[92] Beck C and Cohen E G D 2003 Superstatistics *Physica* A **322** 267

[93] Mura A and Pagnini G 2008 Characterizations and simulations of a class of stochastic processes to model anomalous diffusion *J. Phys. A: Math. Theor.* **41** 285003

[94] Massignan P, Manzo C, Torreno-Pina J A, García-Parajo M F, Lewenstein M and Lapeyre G J Jr 2014 Nonergodic subdiffusion from Brownian motion in an inhomogeneous medium *Phys. Rev. Lett.* **112** 150603

[95] Luo L and Yi M 2018 Non-Gaussian diffusion in static disordered media *Phys. Rev.* E **97** 042122

[96] Wang B, Kuo J, Bae S C and Granick S 2012 When Brownian diffusion is not Gaussian *Nat. Mater.* **11** 481

[97] Wang B, Anthony S M, Bae S C and Granick S 2009 Anomalous yet Brownian *Proc. Natl Acad. Sci.* **106** 15160

[98] Wang W, Seno F, Sokolov I M, Chechkin A V and Metzler R 2020 Unexpected crossovers in correlated random-diffusivity processes *New J. Phys.* **22** 083041

[99] Barkai E, Garini Y and Metzler R 2012 Strange kinetics of single molecules in living cells *Phys. Today* **65** 29

[100] Krapf D *et al* 2019 Spectral content of a single non-Brownian trajectory *Phys. Rev.* X **9** 011019

[101] Thapa S, Lomholt M A, Krog J, Cherstvy A G and Metzler R 2018 Bayesian analysis of single-particle tracking data using the nested-sampling algorithm: maximum-likelihood model selection applied to stochastic-diffusivity data *Phys. Chem. Chem. Phys.* **20** 29018

[102] Cherstvy A G, Thapa S, Wagner C E and Metzler R 2019 Non-Gaussian, non-ergodic, and non-Fickian diffusion of tracers in mucin hydrogels *Soft Matter* **15** 2526

[103] Muñoz-Gil G, Garcia-March M A, Manzo C, Martín-Guerrero J D and Lewenstein M 2020 Single trajectory characterization via machine learning *New J. Phys.* **22** 013010

[104] Granik N, Weiss L E, Nehme E, Levin M, Chein M, Perlson E, Roichman Y and Shechtman Y 2019 Single particle diffusion characterization by deep learning *Biophys. J.* **117** 185

[105] Gajda J, Wyłomańska A, Kantz H, Chechkin A V and Sikora G 2018 Large deviations of time-averaged statistics for Gaussian processes *Stat. Probab. Lett.* **143** 47

[106] Thapa S, Wyłomańska A, Sikora G, Wagner C E, Krapf D, Kantz H, Chechkin A V and Metzler R 2020 Leveraging large-deviation statistics to decipher the stochastic properties of measured trajectories *New J. Phys.* **23** 013008